Electronic nematicity in Sr_2RuO_4

Jie Wu[a,1,2], Hari P. Nair[b,1], Anthony T. Bollinger[a], Xi He[a,c], Ian Robinson[a], Nathaniel J. Schreiber[b], Kyle M. Shen[d,e], Darrell G. Schlom[b,e], and Ivan Božović[a,c,3]

[a]Brookhaven National Laboratory, Upton, NY 11973-5000; [b]Department of Materials Science and Engineering, Cornell University, Ithaca, NY 14853; [c]Department of Chemistry, Yale University, New Haven CT 06520; [d]Physics Department, Cornell University, Ithaca, NY 14853; and [e]Kavli Institute at Cornell for Nanoscale Science, Ithaca, NY 14853

Edited by Zachary Fisk, University of California, Irvine, CA, and approved March 25, 2020 (received for review December 10, 2019)

We have measured the angle-resolved transverse resistivity (ARTR), a sensitive indicator of electronic anisotropy, in high-quality thin films of the unconventional superconductor Sr_2RuO_4 grown on various substrates. The ARTR signal, heralding the electronic nematicity or a large nematic susceptibility, is present and substantial already at room temperature and grows by an order of magnitude upon cooling down to 4 K. In Sr_2RuO_4 films deposited on tetragonal substrates the highest-conductivity direction does not coincide with any crystallographic axis. In films deposited on orthorhombic substrates it tends to align with the shorter axis; however, the magnitude of the anisotropy stays the same despite the large lattice distortion. These are strong indications of actual or incipient electronic nematicity in Sr_2RuO_4.

electronic nematicity | strontium ruthenate | molecular-beam epitaxy | angle-resolved transverse resistivity

It has been predicted theoretically that in some unconventional metals the symmetry of the electron fluid can be spontaneously broken, i.e., reduced compared to that of the underlying crystal lattice (1–5). Indeed, transport anisotropy unexpected from the crystal structure has been observed in copper-oxide (6–15), Fe-based (16–19), and heavy-fermions superconductors (20, 21). This situation is frequently referred to as "electronic nematicity." Here, we will use this term as a shorthand for transport anisotropy that predominantly originates from within the electron fluid itself, i.e., from electron–electron interactions.[†] This brings into focus the interplay between unconventional superconductivity, nematicity, and electron correlations.

Our recent study of a prototypical *d*-wave superconductor, $La_{2-x}Sr_xCuO_4$, using the angle-resolved transverse resistivity (ARTR) method (15), revealed that the electric transport in the normal state shows only twofold rotational symmetry ($\mathbf{C_2}$) while the tetragonal crystal lattice has higher, fourfold ($\mathbf{C_4}$) symmetry. This deviation from the canonical Fermi liquid behavior in cuprates has been ascribed to strong electron correlations. It is of fundamental interest to explore how widespread the nematic state is and whether it is linked with unconventional superconductivity. We have chosen to start with Sr_2RuO_4, since it also is an unconventional superconductor, harbors strong electron correlations, and has the same layered-perovskite (K_2NiF_4) structure as $La_{2-x}Sr_xCuO_4$ (22–30). Thus, one wonders whether the normal state of Sr_2RuO_4, from which the superconductivity emerges, also breaks the rotational symmetry of the lattice, or not.

With this motivation, we have synthesized high-quality single-crystal films of (001)-oriented Sr_2RuO_4 by molecular-beam epitaxy (30). The best films are superconducting with critical temperature $T_c \sim 1.5$ K. The films are deposited on (001)-oriented $(LaAlO_3)_{0.29}$—$(SrTa_{1/2}Al_{1/2}O_3)_{0.71}$ (LSAT) and (110)-oriented $NdGaO_3$ substrates.[‡] The film thickness is chosen to be smaller than the critical thickness for the onset of relaxation, so the in-plane lattice constants of the films remain the same as those of the underlying substrate. Since LSAT is tetragonal while $NdGaO_3$ is orthorhombic (31), comparing Sr_2RuO_4/LSAT to Sr_2RuO_4/$NdGaO_3$ enables us to discern the contributions of the lattice distortion to the observed effects. Details on the synthesis as well as the structural and morphological characterization of the films are provided in *SI Appendix*.

To study the nematicity, we have developed a direct and sensitive method, ARTR (15). The lithography pattern we use is depicted in Fig. 1*A*. A total of 36 Hall bars are arranged radially in a "sunbeam" pattern, with $\Delta\phi = 10°$ angles between successive Hall bars. The electric current runs along a Hall bar, while longitudinal or transverse voltages are measured using three pairs of evenly spaced gold contacts, Fig. 1*B*. The angle $\phi = 0°$ corresponds to the [100] direction of the Sr_2RuO_4 lattice. As explained in ref. 15, if the crystal and the electron fluid both have tetragonal ($\mathbf{C_4}$) symmetry in-plane, the longitudinal resistivity ρ must be isotropic, and the transverse resistivity ρ_T must be zero by symmetry at every angle. In contrast, if the symmetry of the electron transport is reduced to $\mathbf{C_2}$, ρ_T must be nonzero except when the current flow is along one of the principal axes of the electrical conductivity tensor. More precisely, both ρ and ρ_T must oscillate as a function of ϕ with the period of 180°, as follows:

Significance

We have synthesized high-quality thin films of the unconventional superconductor Sr_2RuO_4 on various substrates using molecular-beam epitaxy. We have measured the angle-resolved transverse resistivity (ARTR), a sensitive indicator of electronic anisotropy. The ARTR signal, heralding the electronic nematicity or a large nematic susceptibility, is present and substantial already at room temperature and grows by an order of magnitude upon cooling down to 4 K. In Sr_2RuO_4, an unconventional superconducting state emerges out of an unconventional metallic state.

Author contributions: K.M.S., D.G.S., and I.B. designed research; J.W., H.P.N., A.T.B., X.H., I.R., N.J.S., and I.B. performed research; K.M.S., D.G.S., and I.B. analyzed data; and D.G.S. and I.B. wrote the paper.

The authors declare no competing interest.

This article is a PNAS Direct Submission.

[1]J.W. and H.P.N. contributed equally to this work.

[2]Present address: Department of Physics, Westlake University, 310024 Hangzhou, Zhejiang, People's Republic of China.

[3]To whom correspondence may be addressed. Email: bozovic@bnl.gov.

This article contains supporting information online at https://www.pnas.org/lookup/suppl/doi:10.1073/pnas.1921713117/-/DCSupplemental.

First published May 4, 2020.

[†]This differentiates "electronic nematicity" from transport anisotropy that predominantly originates from the orthorhombicity of the crystal structure, or from formation of a charge density wave that originates from the electron–phonon interaction. In an electronic nematic, both of these effects must be present in principle, but they need not be dominant, and may even be negligible.

[‡]The indices used (also by the substrate vendor) for the $NdGaO_3$ substrate refer to orthorhombic indices (*Pbnm* setting), where the long axis of $NdGaO_3$ is the [001] direction. Similarly, LSAT is referred to with pseudocubic indices even though it is in fact tetragonal, but the distortion is so small that it is difficult to discern and is generally ignored.

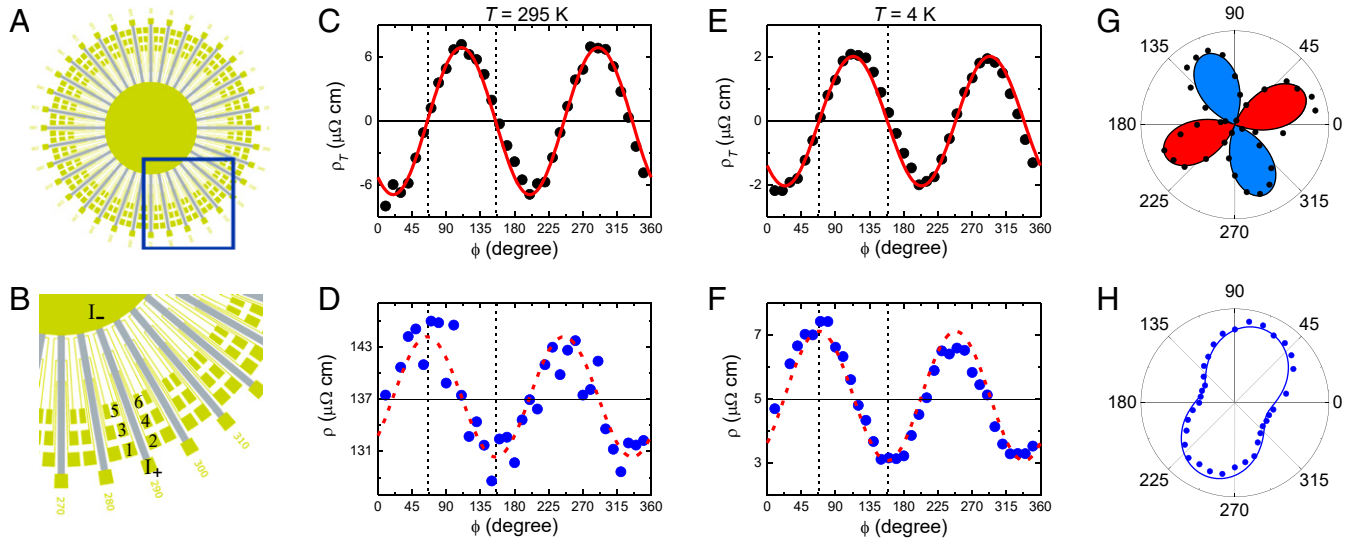

Fig. 1. Angular dependence of the transverse (ρ_T) and longitudinal (ρ) resistivity of the tetragonal Sr_2RuO_4 film on the LSAT substrate. In ultrathin Sr_2RuO_4 films, as determined by the high-resolution X-ray diffraction experiments, the in-plane lattice constants *a* and *b* are epitaxially anchored to those of the substrate. Their difference is tiny (less than 0.03%) in Sr_2RuO_4 grown on tetragonal LSAT substrates. (*A*) A schematic drawing of the lithographic pattern used in this study. Thirty-six identical Hall bars are drawn in steps of $\Delta\phi = 10°$ to cover the whole range from 0 to 360°. (*B*) On each Hall bar, the current runs from the contact I+ to the contact I–. The longitudinal voltages are recorded using pairs like {1,3} and {3,5}, and the transverse voltages using the pairs {1,2}, {3,4}, and {5,6}. The film thickness is 23 nm, the width of each strip is 100 μm, and the voltage contacts are spaced 300 μm apart. (*C*) The measured transverse resistivity ρ_T (black dots) at $T =$ 295 K fits well (the solid red curve) to $\rho_T(\phi) = \rho_T{}^0\sin[2(\phi-\alpha)]$, with $\alpha = 65°$. The black dashed lines mark the angles at which $\rho_T(\phi)$ cross zero. (*D*) The measured longitudinal resistivity $\rho(\phi)$ (blue dots) at $T = 295$ K is well reproduced (the dashed red line) by shifting the fit $\rho_T(\phi)$ curve upward by a constant, $\bar{\rho}$, and left by 45°. The black dashed lines are aligned with those in *C* and correspond to the angles at which $\rho(\phi)$ manifests maximum or minimum values, evidencing the correlation between $\rho_T(\phi)$ and $\rho(\phi)$. (*E*) The same as in *C* but for $T = 4$ K. (*F*) The same as in *D* but for $T = 4$ K. (*G*) The same as in *E*, but plotted in polar coordinates; the experimental data (black dots) and the fit curve (the solid line). Blue filling indicates positive and red negative values. (*H*) The same as in *F*, in polar coordinates.

$$\rho(\phi) = \bar{\rho} + \Delta\rho\cos[2(\phi - a)], \quad [1]$$

$$\rho_T(\phi) = \rho_T^0\sin[2(\phi - a)], \quad [2]$$

where $\bar{\rho} = (\rho_{max} + \rho_{min})/2$, the largest resistivity ρ_{max} is measured along the "hard" axis oriented at some angle α, the smallest resistivity ρ_{min} is measured along the "easy" axis at $\phi = \alpha \pm 90°$, and $\rho_T{}^0 = \Delta\rho = (\rho_{max} - \rho_{min})/2$.

Hence, by measuring $\rho_T(\phi)$ one can detect the breaking of the fourfold symmetry of Sr_2RuO_4. Note that while $\rho(\phi)$ oscillates around some average value $\bar{\rho}$ that can be large, $\rho_T(\phi)$ oscillates around zero and is thus free of such a background signal. This makes the ARTR measurements much more sensitive to the electronic nematicity; its signal-to-noise (limited by the inevitable device-to-device variations due to lithography) is typically better than that of measurements of $\rho(\phi)$ by about 2 orders of magnitude. This ARTR method has substantial advantages compared to just measuring the longitudinal resistivity ρ_a and ρ_b along the two in-plane crystallographic directions, e.g., [100] and [010]. This is best illustrated by an example where the easy axis is diagonal, $\alpha = 45°$. Then one would measure $\rho_a = \rho_b = \bar{\rho}$ and conclude that the sample is isotropic, even if ρ_{max} and ρ_{min} in fact differ by orders of magnitude. In any case, the angular resolution is crucial for determining the principal axes of the resistivity tensor in the event that the tetragonal symmetry is broken and the in-plane resistivity is no longer isotropic. Note that if the symmetry is reduced to orthorhombic, the principal axes of the resistivity tensor must still be aligned with the crystallographic axes, but for lower symmetries are no longer constrained. Importantly, the current flow in the sunbeam pattern is guided in the direction defined by the in-plane orientation of the Hall bar. This is not the case in, e.g., the van der Pauw method (32) where the current flow pattern gets distorted toward the easy axis; this complicates the analysis and can easily produce spurious sign reversals of the ρ_a/ρ_b ratio, as we illustrate in *SI Appendix*.

Our measurements made with the ARTR technique are inconsistent with the fourfold symmetry Sr_2RuO_4 is believed to possess (33). Indeed, they violate Neumann's principle that the macroscopic properties of a perfect crystal must have at least the point-group symmetry of that crystal (34, 35). In Fig. 1 *C* and *E*, we show the ARTR data taken from a Sr_2RuO_4/LSAT sample at temperatures $T = 295$ K and $T = 4$ K, respectively. In both cases, and at every temperature in between, $\rho_T(\phi)$ oscillates with the period of 180° in ϕ, with the sign alternating between positive and negative. All of the experimental data of $\rho_T(\phi)$ (solid dots) can be well fit (the solid red curves in Fig. 1 *C* and *E*) by the simple expression **[2]** with only two free parameters, the amplitude $\rho_T{}^0$ and the phase offset α. In Fig. 1 *D* and *F*, we show the corresponding $\rho(\phi)$ data (blue solid dots). The red dashed curves are not independent fits to these $\rho(\phi)$ data; rather, they are calculated using as an input the values of $\rho_T{}^0$ and α inferred from the $\rho_T(\phi)$ data, shifted up by the angle-averaged longitudinal resistivity $\bar{\rho}$ and then left by 45°. Apparently, the angular oscillations in $\rho(\phi)$ and $\rho_T(\phi)$ have the same amplitude and are phase-shifted exactly as predicted by Eqs. **1** and **2**. This is an unambiguous manifestation of anisotropy in the electric transport in the *a*-*b* plane of the Sr_2RuO_4 film.

To make this more intuitive, in Fig. 1 *G* and *H* we plot the same data as in Fig. 1 *E* and *F*, respectively, but in polar coordinates, where the radial distance scales with the $\rho_T(\phi)$ and $\rho(\phi)$ data measured at $T = 4$ K. The patterns show that the symmetry in the electronic transport is $\mathbf{C}_2$, reduced compared to the $\mathbf{C}_4$ symmetry of the lattice. The "cloverleaf" shape in $\rho_T(\phi)$ should not be confused with the *d*-wave gap symmetry in the momentum space; this is just a consequence of the existence of easy and hard transport axes in real space. This is corroborated by the "peanut" shape in $\rho(\phi)$, as seen in Fig. 1*H*.

Comparing the data at $T = 4$ K and $T = 295$ K, it is apparent that $\rho_T{}^0$ varies with T substantially. In contrast, α remains roughly the same: $\alpha = 68°$ at $T = 4$ K and $\alpha = 65°$ at $T = 295$ K. Hence,

the principal axes of the resistivity tensor are fixed in real space regardless of the sample temperature. It is visually clear in Fig. 1 *G* and *H* that the angles at which the values of $\rho_T(\phi)$ or $\rho(\phi)$ peak do not coincide with the crystallographic axes of the Sr_2RuO_4 or the underlying substrate. The fact that the principal axes do not align with the crystallographic axes defies Neumann's principle (34, 35) and rules out the possibility that the observed "nematicity" simply originates in the anisotropy of the Sr_2RuO_4 lattice imposed by epitaxy on a substrate with a twofold rather than a fourfold symmetry axis perpendicular to it.

We have made extensive efforts to minimize the angular oscillations in $\rho_T(\phi)$ and $\rho(\phi)$ that are caused by extrinsic factors, e.g., contact misalignment, film inhomogeneity and imperfections, film thickness variations, etc. In addition to detailed and targeted experiments already performed (15), we have fabricated a sunbeam device out of a conventional metal (Ti), using the same lithography mask and process to further address the concerns about the lithography process and measurement setup. The ARTR measurements on this control sample indeed show the absence of any angular oscillations in $\rho_T(\phi)$ and $\rho(\phi)$ (see *SI Appendix* for details). This clearly shows that the observed angular oscillations must originate from Sr_2RuO_4. On the other hand, the symmetry of the observed patterns (Figs. 1*H* and 2*F*) and the large magnitude of the observed effect eliminate the possibility that they might originate from conceivable small gradients in the film composition or thickness.

To further explore the effects of lattice distortions, for comparison we have also studied Sr_2RuO_4 films epitaxially grown on (110) $NdGaO_3$, a deliberately chosen orthorhombic substrate. The films were thin enough (23 nm) that the Sr_2RuO_4 lattice in this case is forced to be orthorhombic by the commensurate epitaxial strain. The X-ray diffraction experiments, on the same samples on which $\rho_T(\phi)$ and $\rho(\phi)$ were measured, confirmed this expectation (see *SI Appendix* for details). The *a* and *b* lattice constants differ by 0.5% in the $NdGaO_3$ substrate as well as in the Sr_2RuO_4 films grown upon it. In contrast, in the Sr_2RuO_4 film on LSAT the difference is just 0.03%, more than one order of magnitude smaller. ARTR measurements on Sr_2RuO_4/$NdGaO_3$ films also revealed strong angular oscillations with a period of 180° in both $\rho_T(\phi)$ and $\rho(\phi)$ at $T = 4$ K as well as at $T =$ 295 K (Fig. 2 *A*–*D*). Like in the Sr_2RuO_4/LSAT sample, these $\rho_T(\phi)$ and $\rho(\phi)$ oscillations can be simultaneously well fit by Eqs. **1** and **2** at a given temperature. The fits yield $\alpha = 7^{\circ}$ at $T = 4$ K and $\alpha = 6°$ at $T = 295$ K. The plots in polar coordinates (Fig. 2 *D* and *F*) show this more intuitively: the in-plane directions corresponding to ρ_{max} and ρ_{min} are nearly parallel to the Sr_2RuO_4/$NdGaO_3$ crystallographic [100] and [001] directions of Sr_2RuO_4, respectively. Note, however, that we have repeated the growth of Sr_2RuO_4 on (110) $NdGaO_3$ substrates multiple times and found that in some samples the principal axes are not aligned with either of the crystallographic directions (see *SI Appendix* for details). This indicates that the orthorhombic distortion induced in the Sr_2RuO_4 lattice by the epitaxial strain from $NdGaO_3$ is barely at the border of being strong enough to pin the orientation of nematicity in the electron fluid.

Turning the focus on the amplitude of nematic order, we explore how it depends on temperature and on the epitaxially imposed lattice distortion. To facilitate a quantitative comparison, we define the magnitude of the nematicity as $N = \rho_T^0/\overline{\rho}$. In analogy to the Hall angle, *N* has a geometric interpretation; it is equal to the arctangent of the angle between the directions of the electric field and current-density vectors. Thus, *N* is an intrinsic quantity characteristic of every nematic material. We measured *N* continuously as a function of temperature. In both Sr_2RuO_4/LSAT and Sr_2RuO_4/$NdGaO_3$, $N(T)$ increases rapidly as *T* decreases (Fig. 3), implying that the nematic order is strengthened

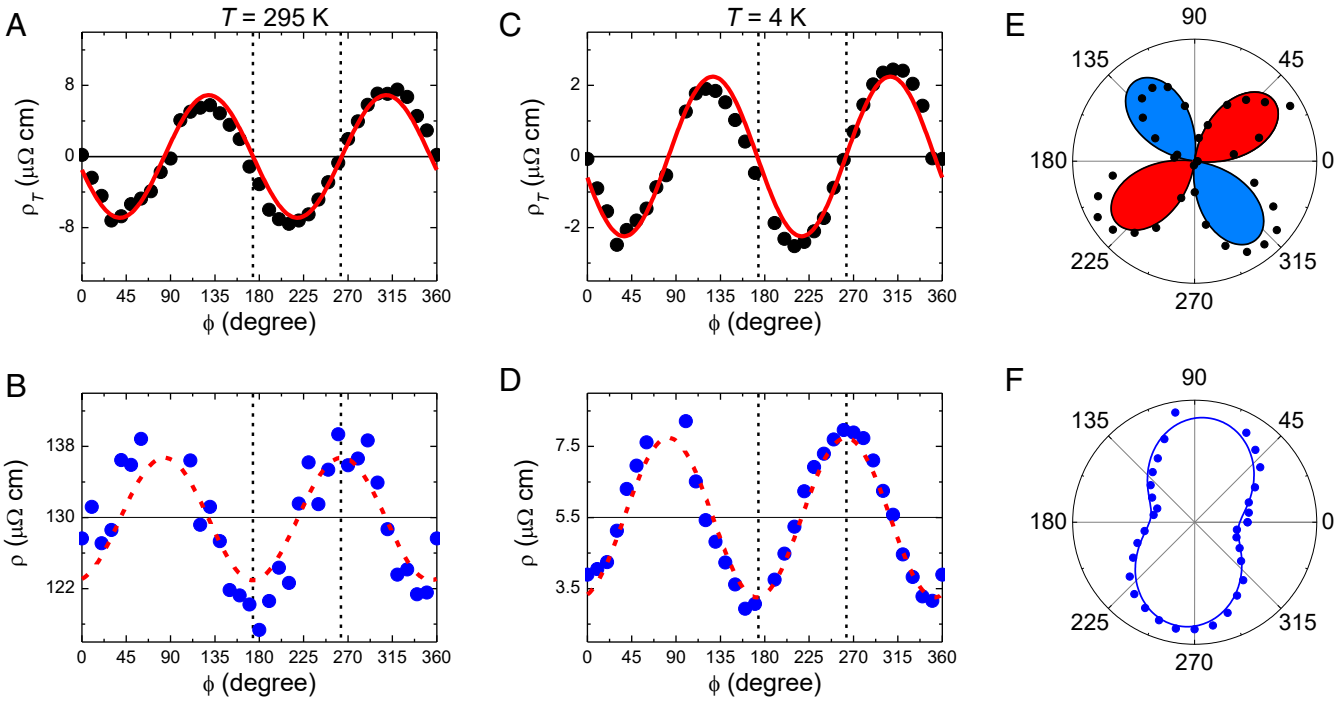

Fig. 2. $\rho_T(\phi)$ and $\rho(\phi)$ of an orthorhombic Sr_2RuO_4 film on a (110) $NdGaO_3$ substrate. In ultrathin Sr_2RuO_4 films grown on orthorhombic (110) $NdGaO_3$ substrates, the difference between *a* and *b* lattice constants is 0.5%, an order of magnitude larger than in Sr_2RuO_4 films on LSAT. (*A*) The $\rho_T(\phi)$ data (black dots) measured at $T = 295$ K and the fit (solid red curve) to $\rho_T(\phi) = \rho_T{}^0\sin[2(\phi-\alpha)]$, with $\alpha = -6°$. The black dashed lines are defined the same way as in Fig. 1. (*B*) The $\rho(\phi)$ data (blue dots) measured at $T = 295$ K are well reproduced (the dashed red line) by the curve obtained by fitting $\rho_T(\phi)$, and shifted upward by a constant, $\overline{\rho}$, and left by 45°. (*C*) The same as in *A* but for $T = 4$ K. (*D*) The same as in *B* but for $T = 4$ K. (*E*) The same as in *C* but plotted in polar coordinates; the experimental data (black dots) and the fit curve (the solid line). Blue filling indicates positive and red negative values. (*F*) The same as in *D*, in polar coordinates.

as the thermal fluctuations diminish. Next, one can see that N is nearly equal in Sr_2RuO_4/LSAT and Sr_2RuO_4/$NdGaO_3$ at every temperature, despite more than an order of magnitude difference between the lattice distortions. If the origin of nematicity were in the anisotropy of the lattice, or of the electron–lattice coupling, N should have increased fast with the lattice distortion, in variance with the experimental observations.

The corresponding temperature-dependent $\rho_T(T)$ and $\rho(T)$, measured at three representative directions, are shown in *SI Appendix*. As the temperature is increased, both $\rho_T(T)$ and $\rho(T)$ increase monotonically. In contrast, $N(T)$ decreases, and one could indeed surmise that it should vanish at some temperature T^*. Unfortunately, this T^* cannot be measured directly since Sr_2RuO_4 films lose oxygen and decompose at elevated temperatures. Nevertheless, it is clear that $N(T)$ deviates significantly from the mean-field–like $(T^*-T)^{1/2}$ dependence; the shape of $N(T)$ is concave instead of convex. Note that the same behavior is seen in $La_{2-x}Sr_xCuO_4$ (15) in $N(T)$ as well as in other key physical parameters such as the upper critical magnetic field H_{c2}, etc., which has been ascribed to the presence of strong fluctuations over a broad T range.

The next important question is how is nematicity related to superconductivity, and more specifically, whether the nematic amplitude traverses through the superconducting transition smoothly or with some jump or kink at T_c. We have addressed this question in three ways. One is that in Sr_2RuO_4 superconductivity is sensitive to uniaxial strain (23). Our Sr_2RuO_4 films are under biaxial strain imposed by the underlying substrate. Although less established, we do observe biaxial strain to affect superconductivity in addition to the other factors described below. The Sr_2RuO_4/LSAT film studied in Fig. 1 is metallic but not superconducting, at least down to $T = 300$ mK, the lowest temperatures available in our Helium-3 cryogenic setup. In contrast, the Sr_2RuO_4/$NdGaO_3$ film studied in Fig. 2 has $T_c \sim 0.9$ K, as shown in *SI Appendix*. Nevertheless, the amplitudes of nematicity are substantial and nearly equal in Sr_2RuO_4/LSAT and Sr_2RuO_4/$NdGaO_3$ (Fig. 3). The other testing opportunity stems from the fact that unlike the superconductivity in conventional metals, the superconductivity in Sr_2RuO_4 is very sensitive to even a minor amount of chemical impurities and other structural imperfections. It was reported that as the residual resistivity of Sr_2RuO_4 increases, T_c decreases sharply to zero (22). Precisely for this reason, it has been an extremely challenging task to synthesize superconducting Sr_2RuO_4 films. Indeed, Sr_2RuO_4 films with the growth conditions even slightly off the optimal growth recipe turn out not to be superconducting. We have thus been able to study, for comparison, an Sr_2RuO_4/$NdGaO_3$ film that has an essentially identical lattice structure and a similar longitudinal resistivity at room temperature as the superconducting film in Fig. 2, but has a somewhat larger residual resistivity and is not superconducting down to $T = 0.3$ K. ARTR measurement on this sample showed $\rho_T(\phi)$ and $\rho(\phi)$ nearly identical to those shown in Fig. 2 (see *SI Appendix* for details) regardless of the differences in disorder and superconductivity. The third way is to suppress the superconductivity by an external magnetic field and show that this underlying metallic state is also nematic, with both $N(T)$ and $\alpha(T)$ seamlessly connecting to their zero-field dependences above T_c. Altogether, the above shows that the nematic state of Sr_2RuO_4 is intrinsic and more robust than superconductivity.

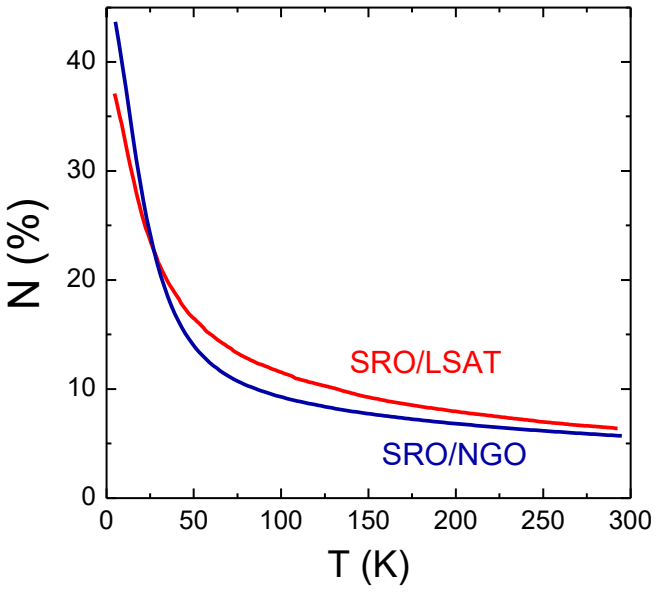

Fig. 3. Temperature dependence of the nematicity magnitude N in the Sr_2RuO_4/LSAT and Sr_2RuO_4/$NdGaO_3$ samples. In analogy to the Hall angle, the magnitude of nematicity is defined as $N = \rho_T^0/\bar{\rho}$. It increases as T decreases in both samples. At any temperature below 300 K, the values of N in Sr_2RuO_4/LSAT and Sr_2RuO_4/$NdGaO_3$ are close to one another, despite the fact that the orthorhombic distortion is more than an order of magnitude larger (0.5%) in Sr_2RuO_4/$NdGaO_3$ than in Sr_2RuO_4/LSAT (0.03%). Apparently, the lattice distortion only affects the principal axes (i.e., the orientation of nematicity) but has almost no effect on the magnitude of the nematicity.

Having established that the resistivity tensor of Sr_2RuO_4 appears to break Neumann's principle based on the established symmetry of Sr_2RuO_4 and the substrates upon which we grew commensurate Sr_2RuO_4 films, we now turn to the question of why? The definite answer would require a quantitative theoretical analysis that is beyond the scope of the present experimental paper, but we can offer some general reflections.

One possibility is that the true symmetry of Sr_2RuO_4 is not tetragonal and that a small distortion exists in it that has not been detected by all prior structural studies. In the structurally related compound, $Sr_3Ru_2O_7$, a structural distortion $\varepsilon = (a - b)/(a + b) \sim 10^{-7}$ that breaks the fourfold symmetry axis below 1.2 K in magnetic fields of 8 T has been detected (36). Such a tiny structural distortion would be below the resolution $\varepsilon \sim 10^{-4}$ of the X-ray techniques used to establish the structure of Sr_2RuO_4 (33). But, for such a small distortion to cause the large anisotropy in transport that we see, the nematic susceptibility, $dN/d\varepsilon$, would have to be very large in Sr_2RuO_4. If that were the case, perhaps some symmetry-breaking defects in Sr_2RuO_4—e.g., such that could arise from step edges that accompany the slight misorientation of the substrates from precisely (001) LSAT and precisely (110) $NdGaO_3$—could lead to a substantial transverse voltage. As described in *SI Appendix*, the substrates used in this study are all oriented within ±0.2°. This together with the extreme sensitivity of superconductivity in Sr_2RuO_4 to disorder implies that the defect concentration of these Sr_2RuO_4 films is small. For standard materials, such minor symmetry breaking from defects would have an imperceptible effect on the measured properties. With a sufficiently large nematic susceptibility, however, this situation can change.

The main problem with the above scenario is that if the nematic susceptibility were very large, one would indeed expect N to grow fast with ε, contrary to what we see—N is nearly the same in Sr_2RuO_4 grown on tetragonal LSAT and orthorhombic NGO substrates, i.e., it seems almost independent of ε.[§]

A more likely option is that for very small ε, $dN/d\varepsilon$ is indeed very large and sufficient to propel the system into a state with a

[§]The same is true in $La_{2-x}Sr_xCuO_4$, as well (15).

substantial transport anisotropy, but once that state is reached, $dN/d\varepsilon$ gets small. Think of a system in a double-well potential, being in unstable equilibrium if it is in the high-symmetry configuration. In this scenario, Sr_2RuO_4 is an electronic nematic over the entire range of our measurements (300 to 4 K). As the temperature is reduced, superconductivity emerges out of the nematic normal state. As for the superconducting state, we have no direct information, since the ARTR technique is "blinded" once the resistance drops to zero, but one can state what seems plausible. The spontaneous breaking of the rotational symmetry in the normal state, as reported here in Sr_2RuO_4, probably indicates that the electron–electron interaction is anisotropic in the *a-b* plane. If that is the case, the rotationally-symmetric *s*-wave superconducting state may be energetically less favorable. Rather, one would expect the strength of Cooper pairing to oscillate with the azimuth angle ϕ, giving rise to a superconducting state with nodes and antinodes along different orientations, like in cuprates.

The experimental status of the symmetry of the superconducting order parameter in Sr_2RuO_4 seems unclear. For many years, Sr_2RuO_4 has been considered as a candidate for *p* wave or more generally for spin-triplet superconductivity (24–28). A recent NMR experiment, however, indicated that the superconducting order parameter of the superconducting state of Sr_2RuO_4 is not odd parity (29), hence, not *p* wave. The results presented here indicate that the *s*-wave state is also unlikely. Taken together, this narrows the options down, and may help resolve this important question.

Yet another option is that in Sr_2RuO_4 there are significant intracell atomic displacements of oxygen ions that break the $\mathbf{C_4}$ symmetry but without affecting the lattice constants. These would be difficult to detect by standard X-ray diffraction techniques, additionally abated by the weak X-ray scattering on oxygen. Then any small external field could favor one direction over the other, and the long-range nature of the Madelung energy could make the single-orientation domains large and/or their distribution strongly imbalanced; this must be the case since we observe anisotropy in transport in our ARTR measurements that probe the sample on the mm scale.

Thus, the present work motivates experiments aimed at resolving among the options listed. One direction would be to study the nematic susceptibility by elastoresistivity measurements (37, 38). If the measurements can be extended down to the 10 mK scale (in a dilution refrigerator), one may even be able to resolve whether $dN/d\varepsilon$ diverges when $T \to T_c$ or when $T \to 0$, if at all; such data would provide critical input to theory, including the exciting proposal that in Sr_2RuO_4 superconductivity may be driven, or enhanced by nematic fluctuations (39, 40). Another, technically challenging but potentially quite illuminating study, would be to directly measure the intracell oxygen displacements in Sr_2RuO_4, if any.

In summary, we believe that the ARTR data reported here in Sr_2RuO_4, and previously in copper-oxide superconductors (15), indicate that the unconventional superconductivity and the nematicity (or a large nematic susceptibility) may be both ascribed to strong and anisotropic electron correlations. We conjecture that electronic nematicity may be widespread in strongly correlated materials, and our ARTR technique provides a direct and simple way for its detection and characterization.

Data and Materials Availability. Data needed to evaluate the conclusions of this manuscript are presented in the main text and *SI Appendix*.

ACKNOWLEDGMENTS. We thank A. Mackenzie and A. Gozar for valuable discussions. The research at Brookhaven National Laboratory was supported by the US Department of Energy, Basic Energy Sciences, Materials Sciences and Engineering Division. X.H. is supported by the Gordon and Betty Moore Foundation's EPiQS Initiative Grant GBMF9074. H.P.N., N.J.S., K.M.S., and D.G.S. acknowledge support from the National Science Foundation (Platform for the Accelerated Realization, Analysis and Discovery of Interface Materials) under Cooperative Agreement DMR-1539918 and from the W.M. Keck Foundation. N.J.S. acknowledges support from the National Science Foundation Graduate Research Fellowship Program under Grant DGE-1650441. This publication is funded in part by the Gordon and Betty Moore Foundation through Grant GBMF9073 to Cornell University. Substrate preparation was performed in part at the Cornell NanoScale Facility, a member of the National Nanotechnology Coordinated Infrastructure, which is supported by the NSF (Grant ECCS-1542081).

1. S. A. Kivelson, E. Fradkin, V. J. Emery, Electronic liquid-crystal phases of a doped Mott insulator. *Nature* **393**, 550–553 (1998).
2. V. Oganesyan, S. A. Kivelson, E. Fradkin, Quantum theory of a nematic Fermi fluid. *Phys. Rev. B Condens. Matter Mater. Phys.* **64**, 195109 (2001).
3. E. Fradkin, S. A. Kivelson, M. J. Lawler, J. P. Eisenstein, A. P. Mackenzie, Nematic Fermi fluids in condensed matter physics. *Ann. Rev. Cond. Mat. Phys.* **1**, 153–178 (2010).
4. E. W. Carlson, K. A. Dahmen, Using disorder to detect locally ordered electron nematics via hysteresis. *Nat. Commun.* **2**, 379 (2011).
5. B. Phillabaum, E. W. Carlson, K. A. Dahmen, Spatial complexity due to bulk electronic nematicity in a superconducting underdoped cuprate. *Nat. Commun.* **3**, 915 (2012).
6. Y. Ando, K. Segawa, S. Komiya, A. N. Lavrov, Electrical resistivity anisotropy from self-organized one dimensionality in high-temperature superconductors. *Phys. Rev. Lett.* **88**, 137005 (2002).
7. V. Hinkov *et al*., Electronic liquid crystal state in the high-temperature superconductor $YBa_2Cu_3O_{6.45}$. *Science* **319**, 597–600 (2008).
8. M. J. Lawler *et al*., Intra-unit-cell electronic nematicity of the high-T_c copper-oxide pseudogap states. *Nature* **466**, 347–351 (2010).
9. R. Daou *et al*., Broken rotational symmetry in the pseudogap phase of a high-T_c superconductor. *Nature* **463**, 519–522 (2010).
10. K. Fujita *et al*., Simultaneous transitions in cuprate momentum-space topology and electronic symmetry breaking. *Science* **344**, 612–616 (2014).
11. Y. Lubashevsky, L. Pan, T. Kirzhner, G. Koren, N. P. Armitage, Optical birefringence and dichroism of cuprate superconductors in the THz regime. *Phys. Rev. Lett.* **112**, 147001 (2014).
12. O. Cyr-Choinière *et al*., Two types of nematicity in the phase diagram of the cuprate superconductor $YBa_2Cu_3O_y$. *Phys. Rev. B Condens. Matter Mater. Phys.* **92**, 224502 (2015).
13. J. Zhang *et al*., Anomalous thermal diffusivity in underdoped $YBa_2Cu_3O_{6+x}$. *Proc. Natl. Acad. Sci. U.S.A.* **114**, 5378–5383 (2017).
14. Y. Sato *et al*., Thermodynamic evidence for a nematic phase transition at the onset of the pseudogap in YBa_2Cu_3Oy. *Nat. Phys.* **13**, 1074–1078 (2017).
15. J. Wu, A. T. Bollinger, X. He, I. Božović, Spontaneous breaking of rotational symmetry in copper oxide superconductors. *Nature* **547**, 432–435 (2017).
16. J.-H. Chu *et al*., In-plane resistivity anisotropy in an underdoped iron arsenide superconductor. *Science* **329**, 824–826 (2010).
17. T.-M. Chuang *et al*., Nematic electronic structure in the "parent" state of the iron-based superconductor $Ca(Fe_{(1-x)}Co_{(x)})_2As_2$. *Science* **327**, 181–184 (2010).
18. R. M. Fernandes, A. V. Chubukov, J. Schmalian, What drives nematic order in iron-based superconductors? *Nat. Phys.* **10**, 97–104 (2014).
19. S. Kasahara *et al*., Electronic nematicity above the structural and superconducting transition in $BaFe_2(As_{(1-x)}P_{(x)})_2$. *Nature* **486**, 382–385 (2012).
20. F. Ronning *et al*., Electronic in-plane symmetry breaking at field-tuned quantum criticality in $CeRhIn_5$. *Nature* **548**, 313–317 (2017).
21. C. M. Varma, L. Zhu, Helicity order: Hidden order parameter in URu_2Si_2. *Phys. Rev. Lett.* **96**, 036405 (2006).
22. A. P. Mackenzie *et al*., Extremely strong dependence of superconductivity on disorder in Sr_2RuO_4. *Phys. Rev. Lett.* **80**, 161–164 (1998).
23. A. Steppke *et al*., Strong peak in T_c of Sr_2RuO_4 under uniaxial pressure. *Science* **355**, 148 (2017).
24. T. M. Rice, M. Sigrist, Sr_2RuO_4: An electronic analogue of ^{3}He? *J. Phys. Condens. Matter* **7**, L643–L648 (1995).
25. Y. Maeno *et al*., Superconductivity in a layered perovskite without copper. *Nature* **372**, 532–524 (1994).
26. A. P. Mackenzie, Y. Maeno, The superconductivity of Sr_2RuO_4 and the physics of spin-triplet pairing. *Rev. Mod. Phys.* **75**, 657–712 (2003).
27. Y. Maeno, S. Kittaka, T. Nomura, S. Yonezawa, K. Ishida, Evaluation of spin-triplet superconductivity in Sr_2RuO_4. *J. Phys. Soc. Jpn.* **81**, 1–29 (2012).
28. A. P. Mackenzie, T. Scaffidi, C. W. Hicks, Y. Maeno, Even odder after twenty-three years: The superconducting order parameter puzzle of Sr_2RuO_4. *Npj Quantum Mater.* **2**, 40 (2017).
29. A. Pustogow *et al*., Constraints on the superconducting order parameter in Sr_2RuO_4 from oxygen-17 nuclear magnetic resonance. *Nature* **574**, 72–75 (2019).
30. H. P. Nair *et al*., Demystifying the growth of superconducting Sr_2RuO_4 thin films. *APL Mater.* **6**, 101108 (2018).

31. M. Steins, J. Doerschel, P. Reiche, Crystal structure of aluminium lanthanum strontium tantalum oxide, $(La_{0.272}Sr_{0.728})(Al_{0.648}Ta_{0.352})O_3$. *Z. Kristallogr. New Cryst. Struct.* **212**, 77 (1997).
32. L. J. van der Pauw, A method of measuring specific resistivity and Hall effect of discs of arbitrary shape. *Philips Res. Rep.* **20**, 220–224 (1958).
33. L. Walz, F. Lichtenberg, Refinement of the structure of Sr_2RuO_4 with 100 and 295 K X-ray data. *Acta Crystallogr. C* **49**, 1268–1270 (1993).
34. W. Voigt, *Lehrbuch der Kristallphysik* (Teubner, Leipzig, 1910), pp. 3–23.
35. J. F. Nye, *Physical Properties of Crystals: Their Representation by Tensors and Matrices* (Oxford University Press, 1985) pp. 20–24.
36. C. Stingl, R. S. Perry, Y. Maeno, P. Gegenwart, Symmetry-breaking lattice distortion in $Sr_3Ru_2O_7$. *Phys. Rev. Lett.* **107**, 026404 (2011).
37. J.-H. Chu, H.-H. Kuo, J. G. Analytis, I. R. Fisher, Divergent nematic susceptibility in an iron arsenide superconductor. *Science* **337**, 710–712 (2012).
38. H.-H. Kuo, J.-H. Chu, J. C. Palmstrom, S. A. Kivelson, I. R. Fisher, Ubiquitous signatures of nematic quantum criticality in optimally doped Fe-based superconductors. *Science* **352**, 958–962 (2016).
39. S. Lederer, Y. Schattner, E. Berg, S. A. Kivelson, Enhancement of superconductivity near a nematic quantum critical point. *Phys. Rev. Lett.* **114**, 097001 (2015).
40. R. M. Fernandes, S. A. Kivelson, E. Berg, Vestigial chiral and charge orders from bidirectional spin-density waves: Application to the iron-based superconductors. *Phys. Rev. B* **93**, 014511 (2016).